Yin *et al. Soft Sci* 2021;1:9
DOI: 10.20517/ss.2021.10

Soft Science

Research Article

Open Access

Check for updates

Control of low dimensionality in flexible hybrid inorganic-organic superlattices

Shujia Yin[1,#], Xin Qian[2,#], Kunihito Koumoto[3,4], Ronggui Yang[2], Chunlei Wan[1]

[1]State Key Laboratory of New Ceramics and Fine Processing, Tsinghua University, Beijing 100084, China.
[2]School of Energy and Power Engineering, Huazhong University of Science and Technology, Wuhan 430074, Hubei, China.
[3]Nagoya Industrial Science Research Institute, Nagoya 464-0819, Japan.
[4]Center of Nanotechnology, King Abdulaziz University, Jeddah 21589, Saudi Arabia.
[#]Authors contributed equally.

Correspondence to: Prof. Ronggui Yang, School of Energy and Power Engineering, Huazhong University of Science and Technology, 1037 Luoyu Road, Wuhan 430074, Hubei, China. E-mail: ronggui@hust.edu.cn; Prof. Chunlei Wan, State Key Laboratory of New Ceramics and Fine Processing, Tsinghua University, 1 Tsinghua Yuan, Beijing 10084, China. E-mail: wancl@mail.tsinghua.edu.cn

How to cite this article: Yin S, Qian X, Koumoto K, Yang R, Wan C. Control of low dimensionality in flexible hybrid inorganic-organic superlattices. *Soft Sci* 2021;1:9. https://dx.doi.org/10.20517/ss.2021.10

Received: 10 Aug 2021 **First Decision:** 19 Aug 2021 **Accepted:** 15 Sep 2021 **First online:** 15 Sep 2021 **Published:** 13 Oct 2021

Academic Editor: Zhifeng Ren **Copy Editor:** Yue-Yue Zhang **Production Editor:** Yue-Yue Zhang

Abstract

The control of electron and phonon transport by manipulating dimensionality is essential for the performance of advanced electronic materials and devices, such as quantum electronics, thermoelectrics and superconductors, which may also lead to yet undiscovered, emergent electronic or thermal phenomena. In this study, we report a series of hybrid inorganic-organic superlattice structures, in which metallic TiS_2 monolayers are spatially confined between soft and insulating organic molecules of varying thicknesses. By choosing different organic molecules that increase the interlayer distance, the electrons inside the TiS_2 layers gradually become two-dimensional, with increasing density of states, as seen by their effective mass that increases from 5.3 to 8.6 m_0, where m_0 is the mass of a bare electron. In addition, density functional theory calculations confirm a transition of the electron distribution from bulk to two-dimensional, due to the suppressed interlayer coupling. This result demonstrates that the thermoelectric transport of two-dimensional electrons can be realized in a three-dimensional inorganic-organic superlattice, thus enabling access to the interesting properties of individual two-dimensional materials in the bulk form, which may provide new opportunities in flexible thermoelectrics.

Keywords: TiS_2, inorganic-organic superlattices, two-dimensional electrons, flexible thermoelectrics

INTRODUCTION

The emergence and popularity of two-dimensional materials (2D) have opened up new opportunities for achieving superb thermoelectric properties compared with their bulk counterparts, as evidenced by tremendous theoretical predictions and some experimental reports[1-8]. However, as the thickness of individual 2D materials is restricted to a few atoms, the maximum heat and current loads allowed through the devices are severely limited, which are not practical for macroscopic thermoelectric applications with energy conversion power at the level of watts. Although there have been many efforts to integrate 2D materials into thick films or three-dimensional (3D) structures, fabrication techniques might introduce undesired doping and defects that compromise electronic properties and lead to the disappearance of the 2D states and their superb properties[9-11]. Realizing the promising thermoelectric properties of 2D materials in a 3D bulk structure is strongly desired for their practical integration into thermoelectric devices with large thermal and electrical loads.

There have been several strategies to realize 2D electronic states in a bulk structure. It was proposed by Hicks and Dresselhaus[12] that confining a conducting thin layer inside insulating layers can result in 2D electrons. The density of states increased, leading to a high Seebeck coefficient and likely an improved thermoelectric performance[12]. This concept was later validated by the observation of the giant Seebeck coefficient in $SrTiO_3/SrTi_{0.8}Nb_{0.2}O_3$ superlattices, where a 2D electron gas (2DEG) can be formed at the interfaces[13]. In contrast, by confining electrons into 2DEGs in $GaN/AlN/Al_{0.2}Ga_{0.8}N$ superlattices, the electron mobility can be greatly enhanced to achieve an improvement in ZT[14]. Meanwhile, 2D materials have been widely recognized to provide a platform in which unconventional pairing states appear in the high-temperature superconductors of layered WTe_2[15] and FeSe[16]. Furthermore, dimensionality-tuned properties have been demonstrated in these layered compounds, with distinctively different critical temperatures T_c being observed in structures with different interlayer spacings[17,18]. Intuitively, a crossover of the transport regime from 3D to 2D can be expected, if the interlayer spacing is changed. Such dimensionality crossover leads to the discovery of novel superconductors, like $Na_xCo_2O_4{\cdot}yH_2O$, where water molecules are inserted between conducting CoO_2 layers[19]. In addition to the effective control of electron transport, phonon transport can also be tailored by dimensionality crossover. Low-dimensional structures appear to have the ability to focus phonons along particular directions leading to ultra-low thermal conductivity[20,21], as well as unusually high thermal conductivity[22].

In our previous work, we studied the thermoelectric properties of bulk inorganic-organic superlattices, in which the inorganic conducting layers were spatially separated by insulating organic layers[23]. Enhanced thermoelectric properties were discovered, together with superior mechanical flexibility. However, 2D electron states and superior thermoelectric properties were not obtained in the hybrid system, as the interlayer distance was limited to 9.65 Å and the interlayer coupling interaction was not decoupled. In this study, by choosing organic molecules of different sizes through a chemical solvent exchange process, the distance between the neighboring inorganic layers is modulated and the insulating organic component can become an electrostatic barrier that confines the electrons inside the inorganic layers. Such intercalation leads to a quantum well structure and 2D transport of charge carriers can be realized in inorganic layers. This dimensionality control is demonstrated by the change in the effective mass of electrons, as well as the electron density distribution as a function of the interlayer distance. Although thermoelectric ZT has not been optimized, this study demonstrates that dimensionality crossover can be achieved in a 3D bulk material, thereby enabling access to the interesting properties of individual 2D materials in the bulk form, which may provide new opportunities in flexible thermoelectrics.

EXPERIMENTAL

We developed an electrochemical processing technique that can be used to synthesize a superlattice structure inside a bulk single crystal. This process opens up the van der Waals gap of a layered material, like TiS_2, through an electrochemical reaction, followed by ion exchange or solvent exchange to diversify and tune the composition.

TiS_2 single crystals with typical dimensions of 4 mm × 4 mm × 100 μm were grown by the chemical vapor transport method using excess sulfur as the transport agent. The hybrid inorganic-organic superlattice compositions were then prepared using an electrochemical process. A TiS_2 single crystal and a platinum plate were used as the cathode and anode, respectively. A solution of hexyl amine (HA) hydrochloride dissolved in dimethyl sulfoxide (DMSO) was used as the electrolyte. The electrochemical reaction was performed under a voltage of 1.8 V for 20 min. Some of the Ti^{4+} ions were reduced to Ti^{3+}. The TiS_2 layer was therefore negatively charged and the positive organic cation in the electrolyte was driven by the Coulombic force. After the intercalation, the thickness of TiS_2 increased to 2.5 times the original thickness. Simultaneously, the uncharged solvent molecules entered the superlattice together due to the cation-dipole effect. The as-synthesized TiS_2/HA/DMSO was then treated in glycerin and H_2O overnight for solvent exchange and cation transfer, respectively. The thickness decreased by ~30% after the solvent exchange with water.

The fabricated hybrid material was then analyzed with X-ray diffraction (XRD) and high-angle annular dark-field scanning transmission electron microscopy (HAADF-STEM). The transport properties of the samples were measured with homemade apparatuses. The Seebeck coefficient was obtained from the slope of the thermovoltage versus temperature gradient. The electrical conductivity was measured by the van der Pauw method. The thermal conductivity was obtained by using the parallel conductance method[24]. All the measurements were calibrated using some reference samples, such as TiS_3 and Mg_2Si, with accuracies within 5%. All the samples were fabricated independently and measured twice or three times to ensure the repeatability of the results. The Hall coefficient was measured using the van der Pauw technique under a reversible magnetic field of 0.5 T (ResiTest8300, Rigaku). The cross-plane thermal conductivity was obtained by multiplying the thermal diffusivity measured by the laser flash analysis method, the heat capacity measured by differential scanning calorimetry and the density calculated by mass over volume.

RESULTS AND DISCUSSION

Chemical and structural analysis of inorganic-organic superlattices

The TiS_2 single crystal is a typical layered transition metal dichalcogenide with a trigonal space group (P-3m1), consisting of a Ti layer sandwiched between two layers of S atoms in an octahedral configuration[25]. Each three-atom slab is stacked with its neighboring layers via relatively weak van der Waals interactions. The prepared hybrid material maintained the same basal plane as that of the TiS_2 single crystal but was expanded along the c-axis. Different from the brittle pristine TiS_2 single crystal, the hybrid superlattices became soft and flexible. For instance, a 54-μm-thick TiS_2/HA/DMSO superlattice sample can still maintain a resistance change of no more than 2% when the bending radius is 2 mm [Supplementary Figure 3].

Structural analysis of the hybrid materials demonstrated the increase of the lattice constant in the c-axis direction, namely, the interlayer distance between the TiS_2 monolayers. The most obvious evidence for the expansion of the interlayer distance came from XRD. The shift of the (00l) peaks reflected the change of the interlayer distance. The (001) peak of bulk TiS_2 is located at 15.5°, corresponding to an interlayer distance of

5.9 Å (as shown in Figure 1A). After the intercalation of the organic molecules, all of the (001) peaks shifted to lower angles.

Despite the fact that the same intercalant (HA) was used, we find that the interlayer distance and thermal stability of the superlattice structures are sensitive to the solvent. When different solvent molecules were exchanged into the superlattices, the corresponding interlayer distance changed accordingly [Supplementary Figure 1]. The interlayer distance for TiS_2/HA/DMSO, TiS_2/HA/glycerin and TiS_2/HA/H_2O were measured to be 13.97, 13.84 and 9.65 Å, respectively. However, the thermal gravimetric analysis showed that TiS_2/HA/DMSO is not stable and decomposes gradually when the sample was heated above 40 ℃ in air. The thermal instability issue can be solved by exchanging solvent molecules with higher boiling point, such as H_2O and glycerin. Thermal stability of the composition of TiS_2/HA/glycerin showed an improvement and remained stable up to 70 ℃. Furthermore, the incorporation of H_2O enabled the hybrid material to remain stable until 120 ℃ in air [Supplementary Figure 2].

We thus examined the structure of the most stable compound TiS_2/HA/H_2O using HAADF-STEM. As shown in Figure 1B, the bright points represent the inorganic TiS_2 layer and the interlayer distance is measured to be 9.65 Å, consistent with the XRD results. The dark area is filled with organic molecules, which support the gaps between inorganic layers. Therefore, the superlattice structure of hybrid inorganic-organic material is confirmed by the HAADF-STEM imaging showing a clear alternating stacking pattern of TiS_2 and organic layers (as shown in Figure 1C).

For the other compositions, TiS_2/HA/DMSO and TiS_2/HA/glycerin, which have lower stability and cannot be observed by HAADF-STEM, the stacking structure of the inorganic-inorganic superlattices can be analyzed with the one-dimensional (1D) electron density map along the c-axis. The 1D electron density maps are derived from the Fourier transform of the XRD results (see supplementary material), as shown in Figures 1D and E. Three sharp peaks located at -1.4, 0 and 1.4 Å represent the triple atomic planes in TiS_2. The organic molecules in the interlayer spacing contributed to the small peaks appearing between the neighboring strong triple peaks, indicating relatively ordered spatial arrangements. The similar peaks next to the triple peaks by 1.4 Å appeared in all the electron density maps, which should belong to the ammonium head groups of HA cations. There are also some relatively strong symmetric peaks located in the interlayer space of the superlattices. These peaks are attributed to the electronegative oxygen and sulfur atoms in the neutral polar molecules, such as DMSO and glycerin, exchanged into the superlattice. Through the cation-dipole effect, they were also regularly arranged between the inorganic layers.

With different sizes of the intercalated molecules, we have demonstrated that the interlayer distance is controllable, indicating excellent opportunities for tunable thermal, electronic and thermoelectric properties. In the following sections, detailed experimental characterization and theoretical analysis are described to demonstrate the dimensionality-controlled thermoelectric transport properties.

Electrical transport properties of inorganic-organic superlattices

The transport properties of TiS_2 single crystal and the hybrid inorganic-organic superlattices were measured, as shown in Table 1. As a result of the high density of electronic states (mainly composed of the three-fold degenerate t_{2g} orbitals of the 3*d* electrons of the Ti atom) around the Fermi level, TiS_2 showed a high Seebeck coefficient and power factor[26]. The transport properties strongly depended on the growth conditions, which might induce nonstoichiometry (interstitial Ti atoms) and other defects[27]. We grew TiS_2 single crystal using excess sulfur rather than conventional iodine as a transport agent to avoid impurities. The obtained TiS_2 single crystals show a Seebeck coefficient of -160 μV K^{-1}, which was lower than that of the

Table 1. Electrical transport properties of TiS_2 single crystals and the hybrid inorganic-organic superlattices

Compositions	T_d	In-plane properties					Cross-plane properties
		S	σ	n	μ	m^*	σ
TiS_2	~	-160	409	3.40	7.24	5.3	0.51
A	40	-75	363	8.48	2.67	8.3	0.14
B	70	-75	534	9.11	3.66	8.6	0.16
C	120	-78	781	7.59	6.41	6.2	2.73

Composition A: TiS_2/HA/DMSO; Composition B: TiS_2/HA/glycerin; Composition C: TiS_2/HA/H_2O; T_d: decomposition temperature in ℃; S: Seebeck coefficient in V K^{-1}; : electrical conductivity in S cm^{-1}; n: the carrier concentration in 10^{20} cm^{-3}; : mobility in cm^2 V^{-1} s^{-1}; m^*: effective mass in m_0, which is the mass of a bare electron.

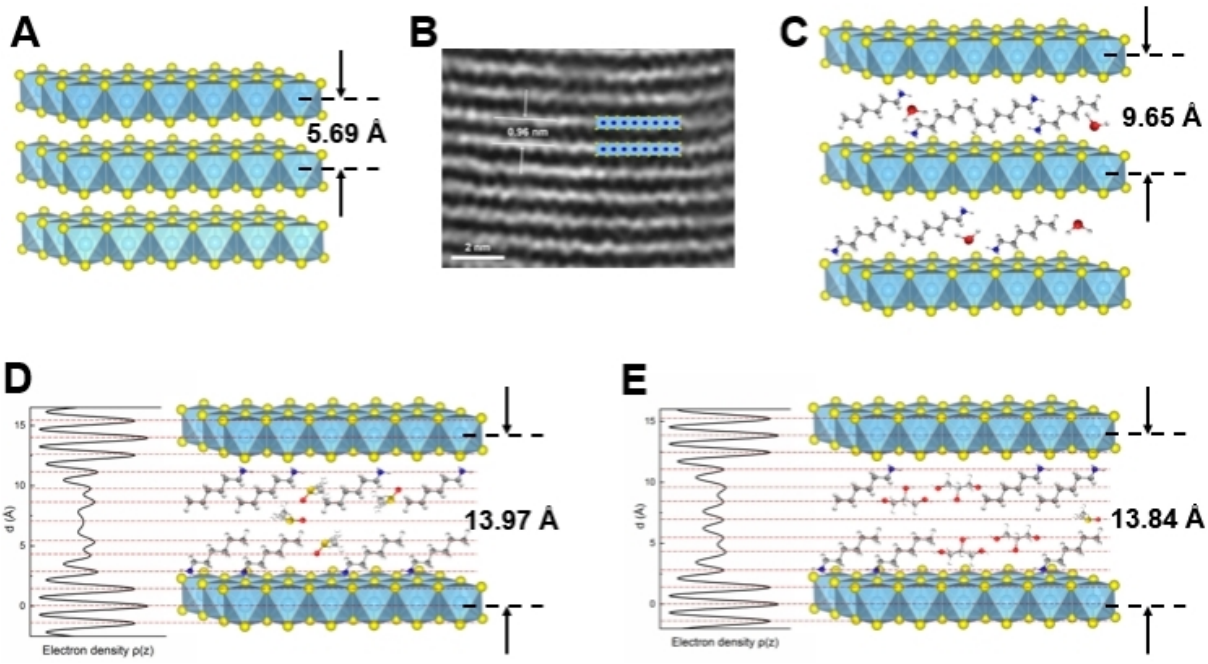

Figure 1. Crystal structures of a TiS_2 single crystal and the hybrid inorganic-organic superlattices with different interlayer distances. (A) TiS_2 single crystal. (B) HAADF-STEM image of TiS_2/HA/H_2O. (C) TiS_2/HA/H_2O. (D) TiS_2/HA/DMSO corresponding to the 1D electron density map along the c-axis. (E) TiS_2/HA/glycerin corresponding to the 1D electron density map along the c-axis.

nearly stoichiometric sample, because of the extra electrons donated by the interstitial Ti atoms. The Hall measurements showed a carrier concentration of 3.4 × 10^{20} cm^{-3}. Assuming that each interstitial Ti atom contributes four electrons, the actual composition of the single crystals was calculated to be $Ti_{1.0049}S_2$.

After the intercalation of HA ions, the Seebeck coefficient became -75 μV K^{-1} and the electrical conductivity became 363 S cm^{-1} at room temperature. During the electrochemical process, the TiS_2 layers were electrochemically reduced, so the carrier concentration in the TiS_2 layers increased and was equal to the density of the intercalated organic cations according to the requirement of charge neutrality. The Hall measurements demonstrated that the carrier concentration increased to 8.48 × 10^{20} cm^{-3}. Meanwhile, the mobility became 2.67 cm^2 V^{-1} s^{-1}, which was reduced compared with that of the TiS_2 single crystal. Since the electrons were primarily localized within the TiS_2 layers and the conduction pathway was well preserved, there should be minimal additional scattering in the inorganic-organic superlattice. The electrons in pure TiS_2 were mainly scattered by acoustic phonons[28], where the electron effective mass also played an

important role. In this quantum well system, the electron effective mass may be changed, which will be analyzed later.

The incorporation of neutral glycerin molecules almost barely changed the concentration of the organic cations (HA ions) and therefore should not influence the electron density in the TiS_2 layers. The electrical conductivity increased from 363 to 534 S cm^{-1}. The Hall measurements showed that this increase was mainly due to an increase in mobility. The polar glycerin molecules with a relatively high dielectric constant in the van der Waals gap of TiS_2 may help screen the deformation potential induced by the lattice vibrations of the TiS_2 layers, which decreased the acoustic phonon scattering effect and enhanced the electron mobility[29].

For the TiS_2/HA/H_2O case, with the highest thermal stability among the three different materials, the Seebeck coefficient exhibits a slight improvement in comparison with the two previous samples. The electrical conductivity was much larger in comparison with the previous two samples. The Hall measurements confirmed that the carrier concentration only slightly decreased, possibly because of a loss of organic cations during the ion exchange process, which can reduce the corresponding negative electron density in the inorganic TiS_2 layers. Meanwhile, the mobility increased to a value close to that of the pristine TiS_2 single crystal.

2D electron transport in inorganic-organic superlattices

Since the intercalated molecules are insulating, the electron pathway is predominantly inside the inorganic TiS_2 layers, likely confined inside the TiS_2 monolayers and determined by the scattering processes inside each TiS_2 layer[28]. Using the volume fraction of the inorganic component derived from the interlayer distance measured by XRD, the real carrier concentration inside the TiS_2 layers can be estimated. The effective mass m^* can then be deduced from the Seebeck coefficient S and the carrier concentration n[30]:

$$S = \frac{8\pi^2 k_B^2}{3eh^2} m^* T \left(\frac{\pi}{3n}\right)^{2/3}$$

The results show that the effective mass of all the inorganic-organic superlattices increased from that of the pristine TiS_2 single crystal, as shown in Figure 2A. The TiS_2 layers are spatially confined between the insulating organic molecules, which can behave as electrostatic potential barriers. A 2DEG could form inside the TiS_2 layers, which increased the density of states at the edge of the conduction band and enhance the effective mass. As shown in Figure 2A, the dimensionality crossover is evidenced by the continuously increased effective mass and decreased mobility with the expanding interlayer distances[31]. Since the insulating organic molecules filling the van der Waals gaps have a much wider bandgap than TiS_2, they can be considered as potential barriers that separate the conducting TiS_2 layers that resemble 2D potential wells. With larger interlayer distances, the width of the potential barriers also increases; hence, the interlayer electron transport is suppressed, resulting in an increased effective mass and decreased mobility. Ultimately, a large spacing leads to a stack of effectively isolated TiS_2 monolayers. Our previous work calculated the electronic structure of the TiS_2 monolayer, in which electrons are completely confined two-dimensionally and the effective mass is doubled compared with the bulk value[1]. The observed increased effective mass from 5.3 m_0 for single crystal TiS_2 to 8.3 m_0 for TiS_2/HA/DMSO with a large interlayer spacing of 13.97 Å suggests we almost approach the monolayer limit.

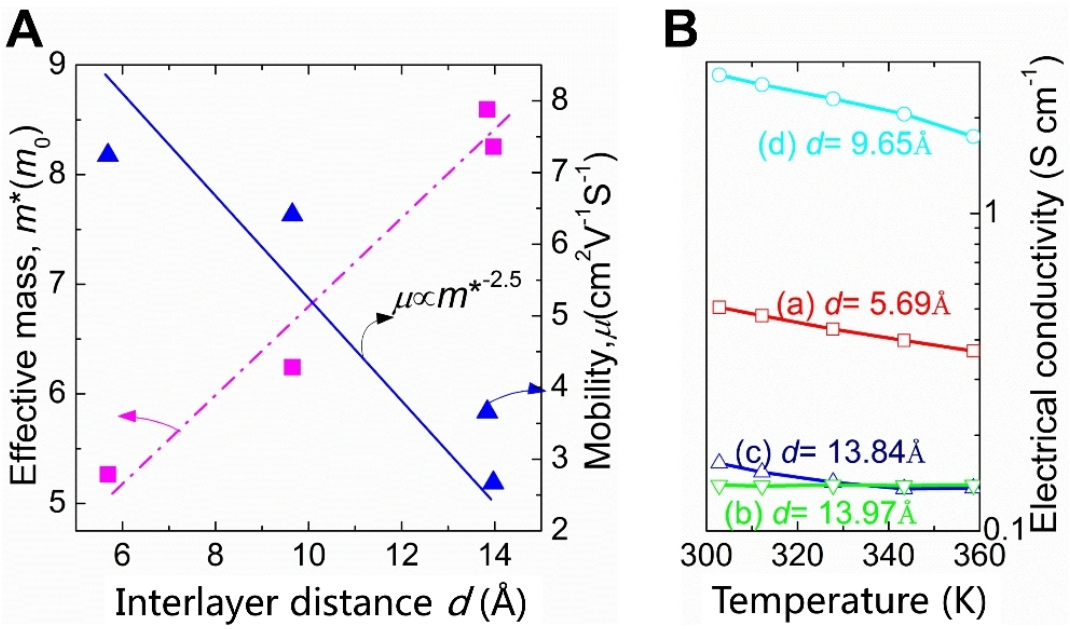

Figure 2. Demonstration of the gradual two-dimensionalization of electrons with increasing interlayer distance. (A) Effective mass and mobility in the in-plane direction as a function of interlayer distance. (B) Temperature dependence of the cross-plane electrical conductivity of the hybrid organic-inorganic superlattices, in which (a-d) represent the TiS_2 single crystal, TiS_2/HA/DMSO, TiS_2 /HA/glycerin and TiS_2/HA/H_2O, respectively.

The formation and the tunability of the 2DEG are also manifested in the temperature dependence of electric conductivity, as shown in Figure 2B. The inorganic-organic superlattices have a highly anisotropic electrical conductivity and the cross-plane electrical conductivities are ~800-2000 times lower than the in-plane values, which can be explained by regarding the organic layers as potential barriers that suppress interlayer charge transport. In addition, the temperature dependence of electrical conductivity for TiS_2/HA/DMSO (d = 13.97 Å) and TiS_2/HA/glycerin (d = 13.84 Å) is much weaker than the pristine TiS_2 and TiS_2/HA/H_2O with smaller interlayer distances. With large widths and heights of potential barriers formed by DMSO and glycerin molecules, the tunneling process dominating the interlayer electron transport is suppressed. In contrast, TiS_2/HA/H_2O has a short interlayer distance and hence the potential barrier is much narrower, resulting in the stronger coupling of charge carriers between neighboring TiS_2 layers and a metallic electrical conductivity in the cross-plane direction. The temperature dependence of electrical conductivity in TiS_2/HA/H_2O is therefore similar to the pristine TiS_2.

In addition to the experimental characterization, we also performed density functional theory (DFT) calculations to provide theoretical insights into the confinement of electron gas inside TiS_2 monolayers by changing the interlayer distances. We calculated the electronic density of states (DOS) of the conduction band as a function of the interlayer distance of TiS_2, as shown in Figure 3. For bulk TiS_2, the DOS at the conduction band edge showed a gradual increase, but the DOS of the monolayer TiS_2 experiences a sharp increase at the band edge, which is a typical feature for a 2DEG. For the structure with intermediate interlayer distances (9.65 and 13.90 Å), the slope of the DOS at the band edge is between the bulk TiS_2 and single layer TiS_2. This DOS clearly showed a bulk-to-2D transition of the electronic structure.

We can also visualize such a transition in the electron distribution from 3D to 2D by calculating the valence electron distributions [Figures 4A-D]. In bulk TiS_2, the electron density clouds of different TiS_2 layers overlap with each other to form a 3D distribution. However, the electrons in each monolayer become

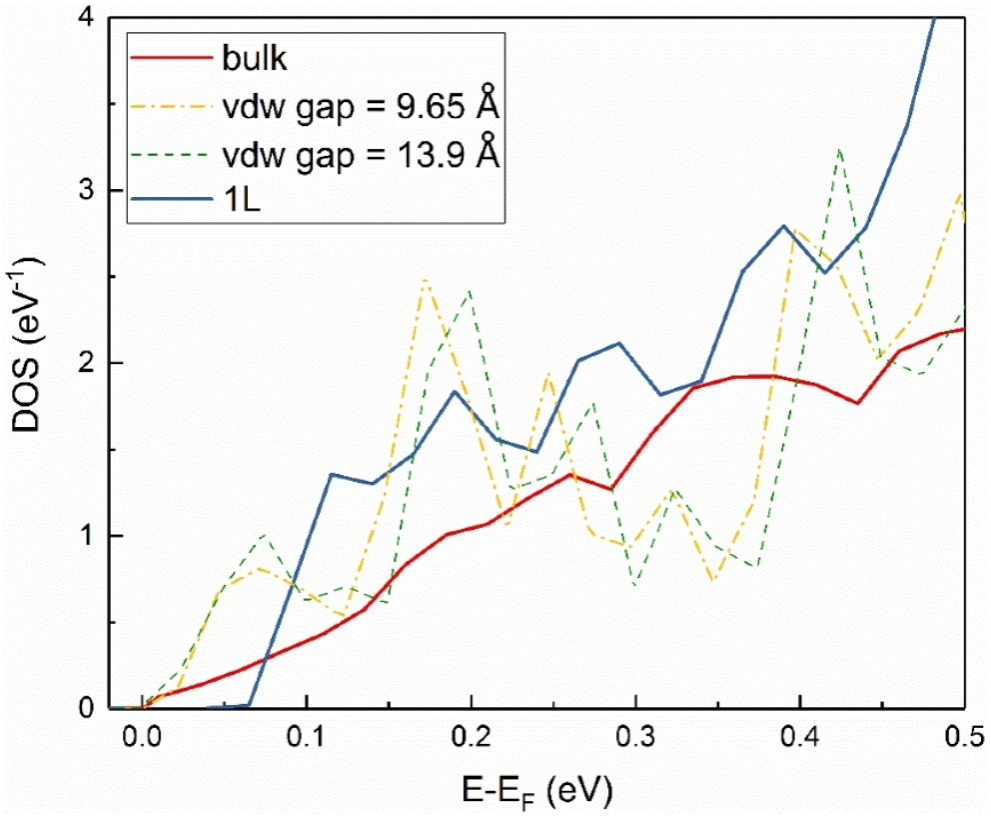

Figure 3. Electronic DOS of the conduction band as a function of the distance between TiS_2 layers.

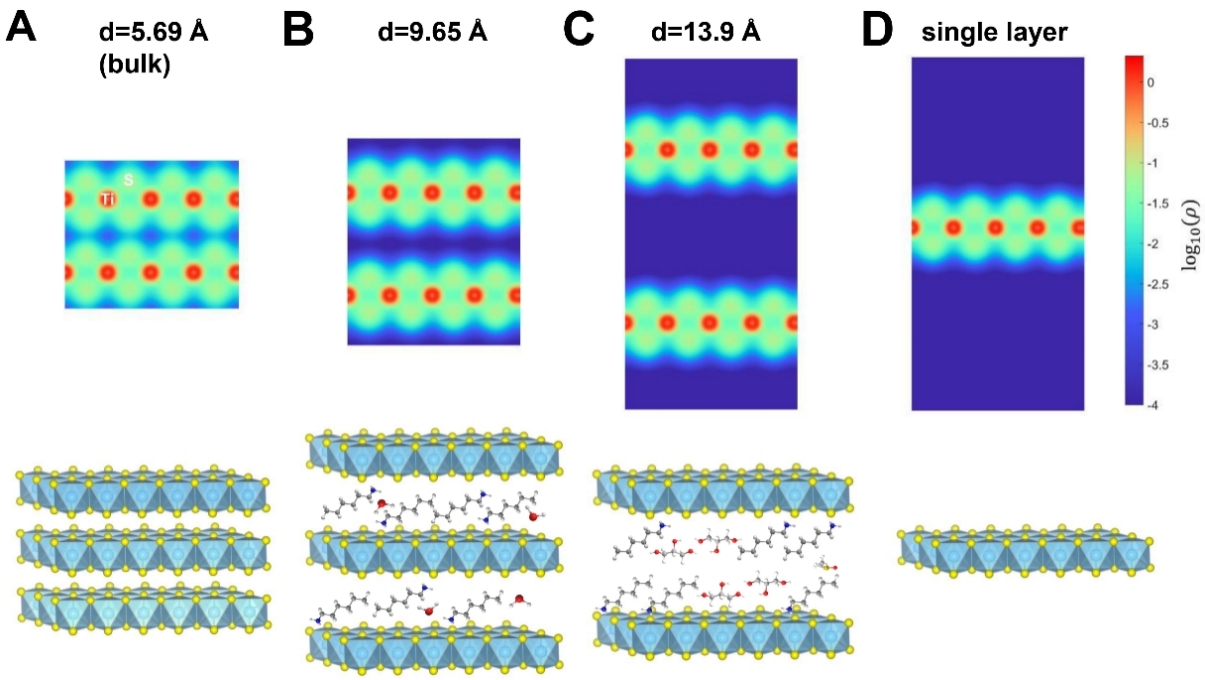

Figure 4. Demonstration of the gradual two-dimensionalization of electrons with increasing interlayer distance. The valence electron distribution of (A) bulk TiS_2, (B) TiS_2 with a van der Waals gap of 9.65 Å, (C) TiS_2 with a van der Waals gap of 13.9 Å and (D) single layer TiS_2.

decoupled from the neighboring layers when the interlayer distance increases. Our DFT simulations of the DOS and the spatial electron density distribution indicate that increasing the van der Waals gap between the TiS_2 layers can suppress the interlayer coupling and the electron transport in these intercalated compounds gradually becomes 2D-like.

Thermoelectric performance as a function of interlayer distance

It is important to realize that careful control of the interlayer spacing is important to avoid excessive reduction of the electrical conductivity that compromises the thermoelectric performance. While opening the van der Waals gaps between TiS_2 layers can enhance the effective mass of electrons, it does not always improve the power factor, because the loss in mobility could counterbalance the gain in the Seebeck coefficient. In addition, the large volume fraction of the insulating organic molecules also decreases the electrical conductivity.

In addition to the electrical properties, increasing the van der Waals gap by organic molecule intercalation can result in much lower phononic thermal conductivities and thereby an enhanced ZT value. Through the parallel thermal conductance method, the thermal conductivity of the pristine TiS_2 single crystal was measured to be 4.45 W m^{-1} K^{-1} along the in-plane direction. The corresponding values for TiS_2/HA/DMSO, TiS_2/HA/glycerin and TiS_2/HA/H_2O were measured to be 0.76, 0.83 and 0.69 W m^{-1} K^{-1}, respectively, which were about six times lower than that of the starting TiS_2 single crystal [Table 2].

As the thermal conductivity is contributed to by both phonons and electrons, the Wiedemann-Franz law was used to estimate the electronic thermal conductivity[32]. The lattice thermal conductivity of the TiS_2 single crystal was calculated to be 4.24 W m^{-1} K^{-1} and the values for the three compositions become 0.22-0.54 W m^{-1} K^{-1}, which were significantly lower than the value of TiS_2. The huge reduction of the thermal conductivity from pure TiS_2 to the hybrid materials is because of the interaction between TiS_2 and the dangling organic molecules, which provides extra scattering channels for TiS_2 vibrational modes, as shown in our previous work using molecular dynamics simulations[23]. Meanwhile, the thermal conductivity of TiS_2/HA/H_2O is lower than the other two hybrid materials, which may be due to the distorted and wavy structure, as shown in Supplementary Figure 4. This wavy structure may be due to the strong interaction between TiS_2 and the organic molecules that are confined within a narrow space (Δd = 3.75 Å). Owing to the significant decrease in thermal conductivity, the ZT value of the hybrid inorganic-organic superlattices achieved a remarkable improvement compared with the TiS_2 single crystal. In general, the thermoelectric properties of the inorganic-organic superlattice change with the change in the interlayer distance [Figure 5].

The cross-plane thermal conductivity was measured using the laser flash method. The electronic thermal conductivity can be neglected compared with the lattice thermal conductivity because of the low cross-plane electrical conductivity. As shown in Table 2, TiS_2 shows anisotropy of thermal conductivity due to the anisotropic bonding strengths: strong covalent bonding inside the layers and weak van der Waals force between the layers. However, this anisotropy ratio between in-plane and cross-plane thermal conductivity decreased after the organic molecule intercalation. This could be attributed to the increased scattering rates of vibrational modes inside TiS_2 due to the anharmonic coupling with the organic molecules, which was demonstrated by molecular dynamics simulations in our previous work[23].

CONCLUSIONS

In summary, we presented a series of materials with a hybrid organic-inorganic superlattice structure, in which the inorganic conducting TiS_2 layers are spatially confined between soft organic molecules. The interlayer distance was systematically tuned by different organic molecules from 9.65-13.96 Å. Gradual

Table 2. Thermal transport and thermoelectric properties of TiS_2 single crystal and the hybrid inorganic-organic superlattices

Compositions	Cross-plane properties		In-plane properties			
	κ	κ_L	$S^2\sigma$	κ	κ_L	ZT
TiS_2	1.92	1.92	1.05	4.45	4.24	0.07
A	0.50	0.50	0.20	0.76	0.54	0.08
B	0.49	0.49	0.30	0.83	0.51	0.11
C	0.11	0.11	0.48	0.69	0.22	0.21

Composition A: TiS_2/HA/DMSO; Composition B: TiS_2/HA/glycerin; Composition C: TiS_2/HA/H_2O; $S^2\sigma$: power factor in mW m^{-1} K^{-1}; : thermal conductivity in $Wm^{-1}K^{-1}$; $_L$: lattice thermal conductivity in W m^{-1} K^{-1}; *ZT*: the dimensionless figure of merit.

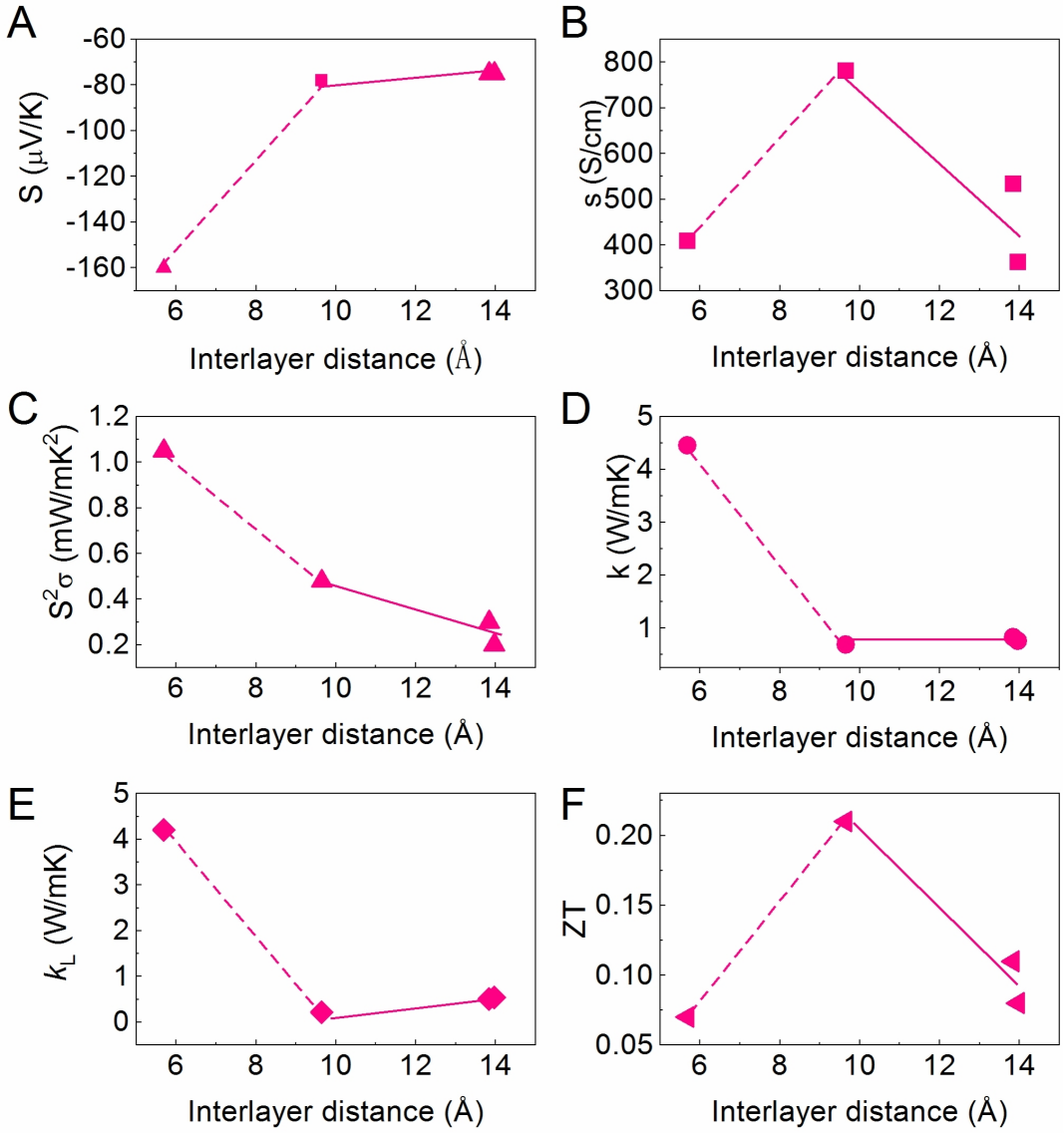

Figure 5. In-plane thermoelectric properties of TiS_2 and the hybrid inorganic-organic superlattices as a function of interlayer distance.

dimensional crossover of the electrons from 3D to 2D was demonstrated with increasing interlayer distance, which was evidenced by the increase of effective mass from 5.6 to 8.3 m_0. Meanwhile, the electron

distribution was analyzed through DFT calculations, which confirm the dimensional crossover of electrons with increasing interlayer distance.

Atomically thin 2D materials show excellent potential in thermoelectric energy conversion due to their superb electronic properties, but the higher thermal conductivities of 2D materials could lead to a low thermoelectric figure of merit[33]. The result demonstrates that thermoelectric transport of 2D electrons can be realized in a 3D inorganic-organic superlattice, thus enabling access to the interesting properties of individual 2D materials in the bulk form, which may provide new opportunities in flexible thermoelectrics. Many other layered materials, such as Bi_2Te_3 and the transition metal dichalcogenides NbS_2, TaS_2, VS_2, CrS_2, MoS_2 and WSe_2, can be intercalated to make both n- and p-type inorganic-organic superlattices materials and realize potentially high thermoelectric properties.

DECLARATIONS

Authors' contributions

Wrote and reviewed the manuscript: Yin SJ, Qian X, Koumoto K, Yang RG, Wan CL

Availability of data and materials

Not applicable.

Financial support and sponsorship

This work was supported by the China Key National R&D Plan (No. 2017YFA0700705) and the National Natural Science Foundation of China (No. 51788104 and No. 51590893).

Conflicts of interest

All authors declared that there are no conflicts of interest.

Ethical approval and consent to participate

Not applicable.

Consent for publication

Not applicable.

REFERENCES

1. Zhang RZ, Wan CL, Wang YF, Koumoto K. Titanium sulphene: two-dimensional confinement of electrons and phonons giving rise to improved thermoelectric performance. *Phys Chem Chem Phys* 2012;14:15641-4. DOI PubMed
2. Huang W, Luo X, Gan CK, Quek SY, Liang G. Theoretical study of thermoelectric properties of few-layer MoS2 and WSe2. *Phys Chem Chem Phys* 2014;16:10866-74. DOI PubMed
3. Hippalgaonkar K, Wang Y, Ye Y, et al. High thermoelectric power factor in two-dimensional crystals of $\mathrm{Mo}{\mathrm{S}}_{2}$. *Physical Review B* 2017;95:115407. DOI
4. Wu J, Chen Y, Wu J, Hippalgaonkar K. Perspectives on thermoelectricity in layered and 2D materials. *Advanced Electronic Materials* 2018;4:1800248. DOI
5. Kayyalha M, Maassen J, Lundstrom M, Shi L, Chen YP. Gate-tunable and thickness-dependent electronic and thermoelectric transport in few-layer MoS2. *Journal of Applied Physics* 2016;120:134305. DOI
6. Pallecchi I, Manca N, Patil B, Pellegrino L, Marré D. Review on thermoelectric properties of transition metal dichalcogenides. *Nano Futures* 2020;4:032008. DOI
7. Shimizu S, Shiogai J, Takemori N, et al. Giant thermoelectric power factor in ultrathin FeSe superconductor. *Nat Commun* 2019;10:825. DOI PubMed PMC
8. Cao YD, Sun YH, Shi SF, Wang RM. Anisotropy of two-dimensional ReS2 and advances in its device application. *Rare Metals* 2021. DOI

9. Novak TG, Kim K, Jeon S. 2D and 3D nanostructuring strategies for thermoelectric materials. *Nanoscale* 2019;11:19684-99. DOI PubMed
10. Huang H, Cui Y, Li Q, et al. Metallic 1T phase MoS2 nanosheets for high-performance thermoelectric energy harvesting. *Nano Energy* 2016;26:172-9. DOI
11. Li D, Gong Y, Chen Y, et al. Recent progress of two-dimensional thermoelectric materials. *Nanomicro Lett* 2020;12:36. DOI PubMed PMC
12. Hicks LD, Dresselhaus MS. Effect of quantum-well structures on the thermoelectric figure of merit. *Phys Rev B Condens Matter* 1993;47:12727-31. DOI PubMed
13. Ohta H, Kim S, Mune Y, et al. Giant thermoelectric Seebeck coefficient of a two-dimensional electron gas in SrTiO3. *Nat Mater* 2007;6:129-34. DOI PubMed
14. Sztein A, Bowers JE, DenBaars SP, Nakamura S. Polarization field engineering of GaN/AlN/AlGaN superlattices for enhanced thermoelectric properties. *Applied Physics Letters* 2014;104:5. DOI
15. Zhang H, Rousuli A, Shen S, et al. Enhancement of superconductivity in organic-inorganic hybrid topological materials. *Science Bulletin* 2020;65:188-93. DOI
16. Shi MZ, Wang NZ, Lei B, et al. FeSe-based superconductors with a superconducting transition temperature of 50 K. *New Journal of Physics* 2018;20:123007. DOI
17. Harshman DR, Mills AP Jr. Concerning the nature of high-Tc superconductivity: Survey of experimental properties and implications for interlayer coupling. *Phys Rev B Condens Matter* 1992;45:10684-712. DOI PubMed
18. Burrard-Lucas M, Free DG, Sedlmaier SJ, et al. Enhancement of the superconducting transition temperature of FeSe by intercalation of a molecular spacer layer. *Nat Mater* 2013;12:15-9. DOI PubMed
19. Takada K, Sakurai H, Takayama-Muromachi E, Izumi F, Dilanian RA, Sasaki T. Superconductivity in two-dimensional CoO2 layers. *Nature* 2003;422:53-5. DOI PubMed
20. Qian X, Zhou J, Chen G. Phonon-engineered extreme thermal conductivity materials. *Nat Mater* 2021;20:1188-202. DOI PubMed
21. Huang Y, Wan C: Controllable fabrication and multifunctional applications of graphene/ceramic composites. *Journal of Advanced Ceramics* 2020;9:271-91. DOI
22. Xu X, Chen J, Zhou J, Li B. Thermal conductivity of polymers and their nanocomposites. *Adv Mater* 2018;30:e1705544. DOI PubMed
23. Wan C, Gu X, Dang F, et al. Flexible n-type thermoelectric materials by organic intercalation of layered transition metal dichalcogenide TiS2. *Nat Mater* 2015;14:622-7. DOI PubMed
24. Zawilski BM, Littleton RT, Tritt TM: Description of the parallel thermal conductance technique for the measurement of the thermal conductivity of small diameter samples. *Review of Scientific Instruments* 2001;72:1770-4. DOI
25. Fang CM, de Groot RA, Haas C. Bulk and surface electronic structure of 1T-TiS2 and 1T-TiSe2. *Physical Review B* 1997; 56:4455-63. DOI
26. Imai H, Shimakawa Y, Kubo Y. Large thermoelectric power factor in TiS2 crystal with nearly stoichiometric composition. *Physical Review B* 2001;64:241104. DOI
27. Barry JJ, Hughes HP, Klipstein PC, Friend RH. Stoichiometry effects in angle-resolved photoemission and transport studies of TI1+XS2. *Journal of Physics C-Solid State Physics* 1983;16:393-402. DOI
28. Wan C, Wang Y, Wang N, Norimatsu W, Kusunoki M, Koumoto K. Intercalation: building a natural superlattice for better thermoelectric performance in layered chalcogenides. *Journal of Electronic Materials* 2011;40:1271-80. DOI
29. Cardona M, Christensen NE. Acoustic deformation potentials and heterostructure band offsets in semiconductors. *Phys Rev B Condens Matter* 1987;35:6182-94. DOI PubMed
30. Snyder GJ, Toberer ES. Complex thermoelectric materials. *Nat Mater* 2008;7:105-14. DOI PubMed
31. Ohta H, Mune Y, Koumoto K, Mizoguchi T, Ikuhara Y. Critical thickness for giant thermoelectric Seebeck coefficient of 2DEG confined in SrTiO3/SrTi0.8Nb0.2O3 superlattices. *Thin Solid Films* 2008;516:5916-20. DOI
32. Kim H-S, Gibbs ZM, Tang Y, Wang H, Snyder GJ. Characterization of Lorenz number with Seebeck coefficient measurement. *APL Materials* 2015:3. DOI
33. Gu XK, Li BW, Yang RG. Layer thickness-dependent phonon properties and thermal conductivity of MoS2. *Journal of Applied Physics* 2016;119:8. DOI